Journal of the Brazilian Society of Mechanical Sciences and Engineering (2023) 45:525
https://doi.org/10.1007/s40430-023-04444-y

TECHNICAL PAPER

Influence of the chemical kinetics on the prediction of turbulent non-premixed jet CH_4 flames

Chunkan Yu[1] · Liming Cai[2] · Lovish Chopra[1,3] · Felipe Minuzzi[4] · Ulrich Maas[1]

Received: 4 May 2023 / Accepted: 22 August 2023
© The Author(s) 2023

Abstract
The present work focuses on the five different chemical mechanisms coupled with *probability density function* (PDF) model to represent the local extinction and re-ignition flame characteristics of the well-known Sandia Flames D–F. These five mechanisms span from the Foundational Fuel Chemistry Model (FFCM) mechanism involving 38 species to the Glarborg mechanism involving 150 species. The coupled *computational fluid dynamics* (CFD) and transported-PDF method are used for the turbulence modeling, and the reaction–diffusion manifolds (REDIMs) are used as an advanced technique for the simplification of chemical kinetics and to speed up the numerical computation. It is demonstrated that these chemical mechanisms have an ability to represent the degree of local extinction and re-ignition accurately. Furthermore, the sensitivity analysis shows that the degree of local extinction is very sensitive to only several key elementary reactions, and an analysis on the turbulence–chemistry interaction investigates the influence of these elementary reactions.

Keywords Probability density function (PDF) · Turbulent combustion · Reduced chemistry · Methane flame

1 Introduction

The development of an accurate chemical mechanism is a key issue in the numerical simulation for chemical reacting systems. This is because not only the accurate prediction of the thermokinetic quantities (for example species concentrations, temperature, pressure) but also the strong turbulence–chemistry interactions are significantly affected by the modeling of chemical mechanism [1]. The chemical mechanism of fuels has normally been validated extensively against experimental data of fundamental combustion targets such as ignition delay times and flame speeds and species profiles of laminar flames, before being applied in turbulent flame modeling [2, 3].

However, various studies confirmed that the performance of chemical mechanisms in a laminar flame can be different from the one in a turbulent flame. Dasgupta et.al. reported in Ref. [4] based on the simulation of a hydrogen-air turbulent premixed flame that the key elementary reactions that have the most contributions to a laminar flame can be different as those in turbulent flames. Cao and Pope reported in Ref. [1] the behaviors of seven different mechanisms in a CH_4 non-premixed turbulent jet flames. They found out that although the Smooke mechanism is constructed with a good accuracy for the species profile measured in a CH_4 counterflow non-premixed flame [5], it displays a significant inaccuracy in the prediction of the local extinction. Farokhi et.al. reported in Ref. [6] based on the simulation of a CH_4 turbulent flame in a small-scale biomass burner that predictions of thermokinetic states can become less sensitive to reaction mechanism in the regions of equilibrium chemistry condition.

These observations from the literature motivate the present work aiming at answering the following questions:

Technical Editor: Daniel Onofre de Almeida Cruz.

✉ Chunkan Yu
chunkan.yu@kit.edu

1 Institute of Technical Thermodynamics, Karlsruhe Institute of Technology, Engelbert-Arnold-Straße 4, 76131 Karlsruhe, Baden-Württemberg, Germany

2 School of Automotive Studies, Tongji University, Cao'an Road No. 4800, Shanghai 201804, People's Republic of China

3 Concordia University, 1455 De Maisonneuve Blvd., Montreal, QC H3G 1M8, Canada

4 Department of Mathematics, Federal University of Santa Maria, Roraima Av., 1000, Santa Maria, RS 97105-900, Brazil

Published online: 17 September 2023

- Are the prediction uncertainties of chemical mechanisms for laminar flames be correlated with their prediction uncertainties for turbulent flames?
- Whether different chemical mechanisms show a similar degree of local extinction in the turbulent simulation?
- Which of the elementary reactions show large sensitivity with respect to the flame behaviors? Could the key reactions in a turbulent flame be different than in a laminar flame? And how these elementary reactions would change the interaction behavior between the chemical kinetics and turbulent mixing processes?

In the literature, a large number of CH_4 chemical mechanisms have been tested and compared for different combustion configuration such as ignition delay time in homogeneous reactors [7] and laminar flame properties [8–11]. In the present work, five different chemical mechanisms (listed in Table 1) are selected for the turbulent non-premixed CH_4 flames. The mechanisms used here contain different number of species and elementary reactions. While the numerical computation using the Foundational Fuel Chemistry Model (FFCM) [12], the GRI 3.0 [1, 13–15], the reduced version of Sandiego-2016 [16] can be found in literature, the performance of the USCII and Glarborg mechanisms in the turbulent flames has not yet been reported.

This work is structured as follows:

- Section 2 gives the first information on five different well-known chemical mechanisms, focusing on the comparison on laminar non-premixed flame, which is similar to the turbulent flame configuration in later section. The sensitivity analysis will be carried out to have a first insight which elementary reactions are important or unimportant in the laminar case.
- Section 6 focuses on the theory of the transported-PDF method, and its coupling with the CFD simulation.
- Section 4 will give the theory of the reaction–diffusion manifold (REDIM) method [22], a method for reduction of chemical kinetics which will be used for the turbulent flame simulation to speed up the computation. The generated REDIM reduced chemistry, which will be used later in the turbulent flame simulation, will be first validated in the laminar case.
- Section 5 will give a deep investigation on the interaction of turbulent mixing process with chemistry. This analysis stems from the fact that different chemical kinetics can lead to different degree of extinction, and such analysis helps us to understand whether the system state will go to burning state or extinction state.
- Section 6 will give a brief review on the validation of proposed CFD/transported-PDF methodology coupled with REDIM reduced chemistry by means of comparing with experimental measurements of well-known Sandia Flame series [23] and the results using detailed chemistry.
- Section 7 will emphasize on the main results and discussion on the prediction of species concentrations by using five different chemical mechanisms. And the sensitivity analysis will also be performed to check whether those reactions, which are important or unimportant in the laminar case, play also role in the turbulent flame.

Table 1 Chemical mechanisms

Mechanism	# of species/# of reactions	References
FFCM	38/289	[17]
GRI 3.0	53/317	[18]
SanDiego-2016	58/279	[19]
USCII	111/784	[20]
Glarborg	150/1391	[21]

2 Chemical mechanisms and their comparison

In this part, five chemical mechanisms listed in Table 1 will be shortly introduced. Then, they will be tested for a simple laminar non-premixed counterflame configuration, and several species concentrations are compared.

2.1 Chemical mechanisms

Five chemical mechanisms for methane combustion are considered in this study.

- The *GRI 3.0* [18] model was developed by Smith et al. by calibrating its kinetic parameters automatically against the fundamental combustion targets, such as ignition delay times and laminar burning velocities. It has been widely applied in the combustion community in the modeling of oxidation of methane various cases like homogeneous reacting systems and laminar flames in addition to turbulent combustion systems at various conditions.
- The *USCII* [20] model was developed based on the *GRI 3.0* [18] model and contains the high-temperature chemistry of hydrogen, carbon monoxide, and a number of C1–C4 hydrocarbon species, including methane. Since it consists of 111 species, its application in the modeling of turbulent flames is rarely reported.
- The *SanDiego-2016* [19] model was proposed to describe the oxidation of C0–C4 species, such as hydrogen, methane, methanol, ethanol, propane, and *n*-butane. It was

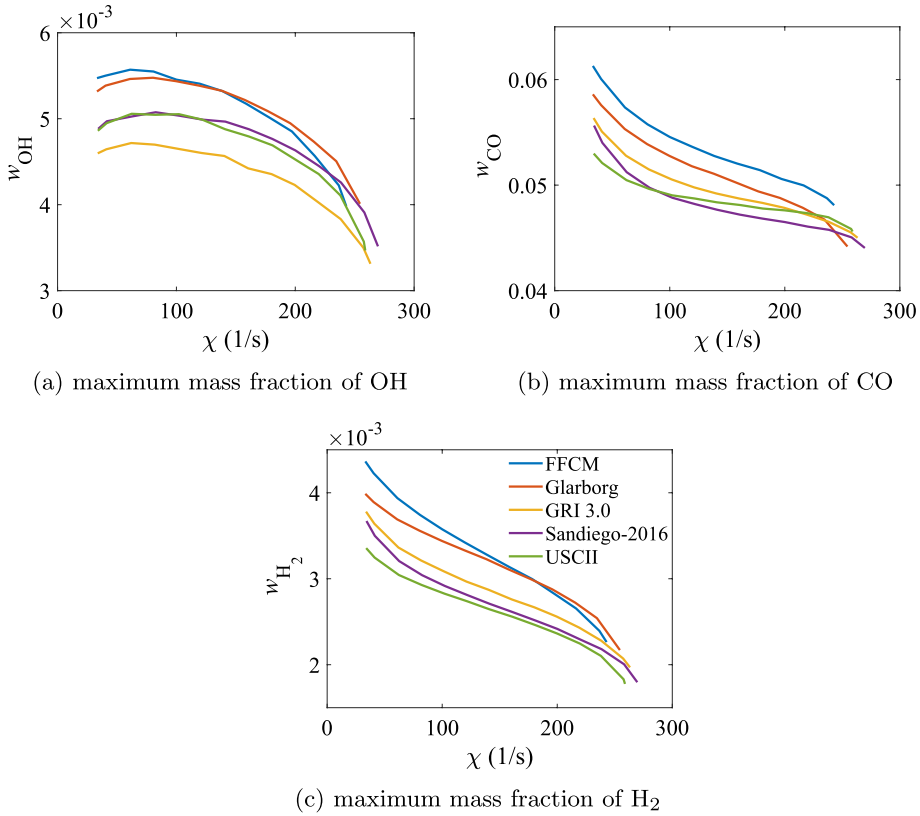

(a) maximum mass fraction of OH (b) maximum mass fraction of CO

(c) maximum mass fraction of H_2

Fig. 1 Comparison of thermokinetic quantities in terms of their maximum values using different chemical mechanisms

Table 2 Arrhenius parameters for selected elementary reactions

Elementary reactions	A	β	E_a
(R1) $H + O_2 = OH + O$	2.650×10^{16}	−0.6707	17041.0
(R2) $CO + OH = CO_2 + H$	4.760×10^{7}	1.228	70.0
(R3) $CH + OH = HCO + H$	3.0×10^{13}	0.0	0.0

Units are cm^3-s-kcal-K, and $k = AT^{\beta}\exp(-E_a/RT)$

derived with a minimum number of species and reactions required to predict the fundamental combustion targets accurately. Its performance on the turbulent flames is reported in Ref. [24].

- The *FFCM* [17] model was developed for the combustion of H_2, H_2/CO, CH_2O, and CH_4 by incorporating up-to-date kinetics and by applying uncertainty quantification method in order to improve its performance. The model was validated successfully against a large set of available combustion data over a wide range of conditions. It has also been used in the modeling of turbulent methane combustion system under general engine-operating conditions. [12].
- The *Glarborg* model [21] was proposed to describe the formation and consumption of nitrogen oxides in the combustion of hydrocarbon fuels, such as methane. In the methane sub-reaction mechanism, the rate constants of the elementary reactions were revised carefully based on a thorough review on the measured and calculated results available in the literature.

Numbers of species and reactions involved in these chemical mechanisms are summarized in Table 1.

2.2 Comparison in a laminar non-premixed counterflow flame configuration

In this part, we provide a short comparison of thermokinetic quantities predicted by these five different chemical mechanisms for a laminar counterflow non-premixed configuration at $p = 1$bar. The gas mixture compositions of both fuel and oxidizer sides are consistent with the one used in Sandia Flame series [23]:

- Left boundary: mixture consists of 25% CH_4 and 75% air by volume; Its temperature is $T = 294$K.
- Right boundary: mixture consists of pure air with temperature $T = 292$K.

In the framework of laminar non-premixed flame, the scalar dissipation rate χ is an important quantity, which is defined as [25]:

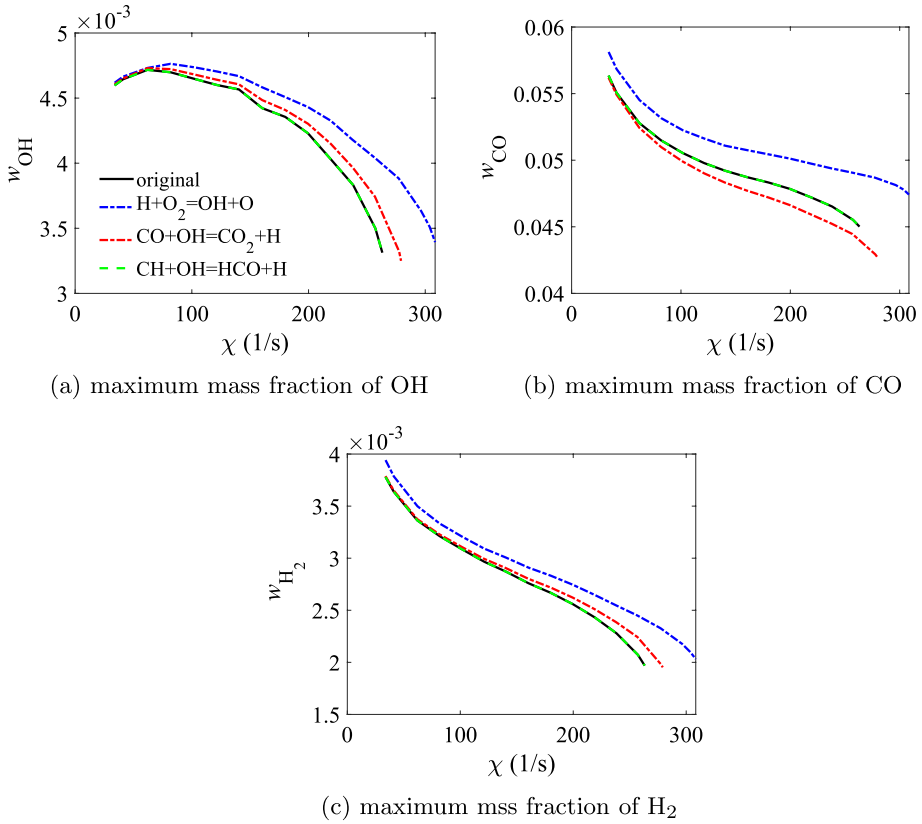

(a) maximum mass fraction of OH

(b) maximum mass fraction of CO

(c) maximum mss fraction of H_2

Fig. 2 Change of selected species concentrations with respect to three different elementary reactions. Color lines: the pre-exponential factor is increased 20% (color figure online)

$$\chi = 2D_{\xi}(\nabla\xi)^2, \tag{1}$$

where ξ is the mixture fraction and D_{ξ} its diffusion coefficient.

The numerical computation is performed using the in-house INSFLA code [26] with the assumption that the Lewis number for all species is unity ($Le_i = 1$). The reason for the use of unity Lewis number assumption is to enable a consistent comparison with the turbulent calculations.

Figure 1 compares the thermokinetic quantities over scalar dissipation rate χ at stoichiometric mixture fraction position. The very right points of the curves are the extinction scalar dissipation rate (χ_E), above which no stable burning flame can be obtained and any burning flame is quenched. Several important observations should be mentioned here before evaluating their performance on the turbulent simulation:

- These mechanisms show similar extinction limit. More precisely, the FFCM mechanism predicts the lowest extinction limit with $\chi_E(\text{FFCM}) = 243\ \text{s}^{-1}$ and the Sandiego-2016 the highest with $\chi_E(\text{Sandiego-2016}) = 270\ \text{s}^{-1}$, and the max. deviation is only around 10%.
- The predicted species mass fractions can differ significantly in the regime where stable burning flames exist. For example, the value of OH mass fraction can differ of order 20% at low scalar dissipation rate regime. This can be attributed to the different formation rate of these species. For example, the FFCM gives the highest formation rate of CO, which resulting in a high CO concentration.

2.3 Sensitivity of non-premixed counterflow flame with respect to reaction rate

An important aspect of modeling investigation on chemical kinetics is the determination of key chemical reactions, which most strongly affect the thermokinetic quantities and non-premixed flame properties such as extinction limit. This can be approached by performing the sensitivity analysis [27]. Therefore, in this part, we examine how sensitive the predicted thermokinetic quantities change with respect to the elementary reactions. Table 2 lists Arrhenius parameters for three selected elementary reactions. The selection follows the fact that (R1) is the most sensitive elementary reaction and (R3) has almost no influence on the flame properties, which is confirmed through the laminar flame speed and flame extinction limit in Refs. [10, 28–30].

The sensitivity study has been performed in the way that the pre-exponential factor for each elementary reaction is increased 20% (1.2A). The effect of these elementary

reactions on the species concentrations and the extinction limit for the laminar system is represented in Fig. 2. Several interesting observations should be addressed here:

- While the selected species concentrations are almost insensitive to the change of the reaction rate of (R3) CH + OH = HCO + H, they are sensitive to (R2) CO + OH = CO_2 + H and significantly affected by the (R1) H + O_2 = OH + O. This is a well-known fact that the (R1) and (R2) are most important. Moreover, it is noticed that the larger the scalar dissipation rate χ is, the more sensitive the species concentrations are.
- As also confirmed in Refs. [10, 28], (R1) H + O_2 = OH + O and (R2) CO + OH= CO_2 + H are the two most sensitive elementary reactions with respect to the extinction limit. Especially for the (R1), the increase of its pre-exponential factor improves significantly the burning stability against extinction limit.

2.4 Some comments on the behaviors of different mechanisms

Based on the performance of these five chemical mechanisms on the laminar non-premixed counterflow flame calculation, several interesting questions can be raised:

- If the chemical mechanisms predict different behaviors of the thermokinetic quantities, will such difference be preserved in the turbulent case?
- If the chemical mechanisms predict similar extinction limit, will these mechanisms also predict the similar degree of local extinction in the turbulent case?
- If the flame properties are sensitive to some key elementary reaction, will the turbulence prediction (e.g., the degree of local extinction) also be sensitive to it?

To answer these questions, numerical simulation for the turbulent reacting systems has to be performed. In the rest of the work, we will only focus on the turbulent simulation. The theory of the turbulence modeling and the chemical kinetic modeling will be discussed. Afterward, the five chemical mechanisms will be applied for the simulation of well-known Sandia Flame series [23].

3 CFD/Transported-PDF models for the simulation of turbulent reacting flows

In the present work, the Reynolds-averaged Navier–Stokes (RANS) coupled with the transported-PDF (TPDF) model is used for the mathematical modeling of the turbulence simulation with chemical kinetics. The used algorithm is consistent with the one proposed by Murodoglu et al. [31] and our previous work [32]. Therefore, only the most important equations are outlined in this work. More details can be found in the corresponding literature references.

3.1 Reynolds-averaged Navier–Stokes (RANS) for the flow field

For the flow field calculations, the Favre-averaging is applied for the governing conservation equations, and accordingly, the Favre-averaged continuity equation and momentum equations for RANS can be written as:

$$\frac{\partial \overline{\rho}}{\partial t} + \frac{\partial}{\partial x_i}\left(\overline{\rho}\widetilde{u_i}\right) = 0, \tag{2}$$

$$\frac{\partial \overline{\rho}\widetilde{u_i}}{\partial t} + \frac{\partial}{\partial x_j}\left(\overline{\rho}\widetilde{u_i}\widetilde{u_j} + \overline{p}\delta_{ij}\right) = -\frac{\partial}{\partial x_j}\left(\overline{\rho}\widetilde{u_i'' u_j''}\right), \tag{3}$$

$$\overline{p} - \overline{\rho}\cdot\widetilde{R_g T} = 0 \tag{4}$$

where $\widetilde{\cdot}$ represents the Favre-averaged values and $\cdot''$ the Favre-fluctuations. Here $u_i = (u_1, u_2, u_3)^{\mathrm{T}}$ is the velocity vector including three velocity components. The term $\overline{\rho}\widetilde{u_i'' u_j''}$ is the unclosed Favre-averaged Reynolds stresses determined from the TPDF model (see Sect. 3.2). δ_{ij} is the Kronecker delta, which equals 1 for $i = j$ and 0 for $i \neq j$. R_g is the mass-specific gas constant defined as $R_g = R/\overline{WM}$ ($\overline{WM}$: molar mass of mixture; $R = 8.314$ J/(mol K): universal gas constant).

In our model, we follow the idea from Ref. [31] that the effect of the flow viscosity (the divergence of deviatoric stress in Eq. (3)) is negligible. Furthermore, there is no need to solve the energy conservation equation in the CFD code as the Favre-averaged temperature $\widetilde{T}$ is determined by the PDF method and can be easily retrieved from the reduced chemistry table.

Table 3 Parameters and their values for each model used in the TPDF method

Parameter	Value	Applied model
C_0	2.1	Simplified Langevin model Eq. (9) [34]
C_Ω	0.6892	Turbulent frequency model in Eqs. (6), (7) and (8c) [41]
$C_{\omega 1}$	0.71	
$C_{\omega 2}$	0.90	
C_3	1.0	
C_4	1.25	
C_ϕ	1.5	EMST-mixing model [37]

3.2 Transported-PDF (TPDF) model

In the present work, a joint *probability density function* (PDF) of velocity-composition-turbulent frequency (VCF-PDF) is employed [31, 33] due to its remarkable advantage: Chemical reactions can be treated in an exact way, without approximation. The derived TPDF equation can be solved numerically by using the Monte-Carlo particle method [34, 35], where the PDF is represented by an ensemble of notional particles with flow and thermokinetic properties (position $\mathbf{x}^*$, velocity fluctuation $\mathbf{u}''^{,*}$, thermokinetic states Ψ^*, and turbulent frequency ω^*) evolving according to stochastic processes [34, 36]. The thermokinetic state Ψ^* in a reacting flow with n_{sp} species can be described by a vector $\Psi = \left(h, p, \phi_1, \ldots, \phi_{n_{sp}}\right)^T$ of $n = n_{sp} + 2$ dimensions, where h and p are the specific enthalpy and pressure, respectively, and ϕ_i is the specific mole fraction of species i, defined as $\phi_i = w_i/WM_i$ (w_i is the mass fraction and WM_i the molar mass of species i).

The evolution of the notional particle's properties is described by the following stochastic differential equations (SDEs) [31, 34, 35]:

- evolution of the particle position x_i^*:

$$\mathrm{d}x_i^* = \left(\widetilde{u}_i + u_j''^{,*}\right)\mathrm{d}t, \tag{5}$$

- evolution of the particle turbulent frequency ω^*:

$$\begin{aligned}\mathrm{d}\omega^* =& -C_3\Omega\left(\omega^* - \widetilde{\omega}\right)\mathrm{d}t - S_\omega\Omega\omega^*\mathrm{d}t \\ &+ \sqrt{2C_3C_4\Omega\widetilde{\omega}\omega^*}\cdot\mathrm{d}W,\end{aligned} \tag{6}$$

where S_ω is the sink of turbulent frequency

$$S_\omega = C_{\omega 2} - C_{\omega 1}\cdot\frac{\mathcal{P}}{k\cdot\Omega}, \tag{7}$$

$\mathcal{P}$ the turbulence production, k the turbulent kinetic energy and Ω the conditionally averaged turbulent frequency:

$$\mathcal{P} = -\widetilde{u_i''u_j''}\cdot\frac{\partial\widetilde{u}_i}{x_j}, \tag{8a}$$

$$k = \frac{1}{2}\widetilde{u_i''u_i''}, \tag{8b}$$

$$\Omega = C_\Omega\cdot\frac{\overline{\rho^*\omega^*|\omega^* \geq \widetilde{\omega}}}{\overline{\rho}}. \tag{8c}$$

- evolution of the particle velocity fluctuation $u_i''^{,*}$:

$$\begin{aligned}\mathrm{d}u_i''^{,*} =& \frac{1}{\overline{\rho}}\frac{\partial\left(\overline{\rho}\widetilde{u_i''u_j''}\right)}{\partial x_j}\mathrm{d}t - u_j''^{,*}\frac{\partial\widetilde{u}_i}{\partial x_j}\mathrm{d}t \\ &- \left(\frac{1}{2} + \frac{3}{4}C_0\right)\Omega u_i''^{,*}\mathrm{d}t + \sqrt{C_0k\Omega}\cdot\mathrm{d}W_i,\end{aligned} \tag{9}$$

- evolution of the particle thermokinetic states Ψ^*:

$$\frac{\mathrm{d}\Psi^*}{\mathrm{d}t} = \mathbf{F}(\Psi^*) + \mathbf{M}, \tag{10}$$

where the terms $\mathbf{F}(\Psi^*)$ and $\mathbf{M}$ are, respectively, the source term of the thermokinetic states and the mixing process. The modeling of the mixing process in the framework of PDF methods plays an important role for the simulation accuracy. Various mixing models with different levels of accuracy and complexity have been developed, ranging from the most simplest Interaction by Exchange with the Mean (IEM) to very complex models such as the Euclidean minimum spanning trees (EMST) [37] and the multiple mapping conditioning (MMC) [38]. A nice review on the discussion about various mixing models can be found in Refs. [39, 40]. In this work, the EMST mixing model is used.

In Table 3, all values of model parameters are listed and used in the present work for the simulation of Sandia Flame series, which is consistent with those used in Ref. [1].

4 Modeling of chemical kinetics

Although the high-performance computing (HPC) allows a numerical simulation using detailed chemical kinetics, the large number of species and reactions involved in

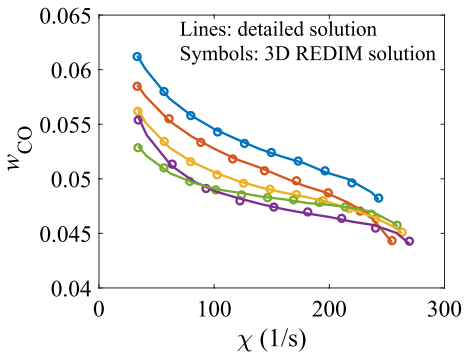

Fig. 3 Comparison of the mass fraction of CO in the non-premixed counterflow flame configuration using the detailed chemistry (solid lines) and the 3D REDIM reduced chemistry (symbols). The colors are consistent with those in Fig. 1 (color figure online)

the detailed chemistry enhances the complexity of turbulence–chemistry interaction and computational effort. For example, Wang et al. used a reduced chemical model derived from GRI 3.0 [17] involving 28 species and 268 reactions in Ref. [42] for the study of turbulent premixed methane/air flames at high Karlovitz number, and the simulation is reported to take approximately 22 days. Therefore, although the use of detailed chemistry provides most reliable results, its large simulation time is less acceptable for engineering application and is only achievable for those detailed chemistry with less than around 60 species, as reported, e.g., in Refs. [43–45]. In order to speed up the numerical computation, the model reduction for chemical kinetics with high accuracy is required. The manifold-based simplified chemistry is one of the class, which is usually expressed as [46, 47]:

$$\mathcal{M} = \{\Psi : \Psi = \Psi(\Theta), \quad \Psi : \mathbb{R}^{m_s} \rightarrow \mathbb{R}^n\}, \tag{11}$$

with Θ the vector of reduced coordinates parametrizing the slow manifold. Candidates within this class are, e.g., the intrinsic low-dimensional manifold (ILDM) [48], laminar flamelet model [49], flamelet-generated manifold (FGM) [50], reaction–diffusion manifolds (REDIM) [22], etc. In Ref. [47], a detailed introduction and overview can be found. Although the simplified chemistry can largely save the computational cost, it must fulfill the requirement that the flame quantities and structures (e.g., species concentrations, extinction limits) must be preserved when using the simplified chemistry. The REDIM model is applied in the present work. After reviewing briefly its theory, it will be examined in the laminar non-premixed counterflow flame configuration, showing its ability to capture the flame quantities and structures.

4.1 Outline of reaction–diffusion manifolds (REDIMs) model

The reaction–diffusion manifolds (REDIMs) method [22] is an advanced reduction technique for the chemical kinetics based on the concept that the thermokinetic states are constrained on the slow manifold with much lower dimension (compared to dimension of full system) due to chemical and physical time-scales differing from orders of magnitude [46, 47]. Unlike other efficient computational tools such as ISAT [51] where reaction mechanisms of only order 50 species can be effectively applied as reported in Ref. [1], there is no restriction on the number of species involving in the reaction mechanisms if the REDIMs method is applied.

A detailed description and implementation of REDIM can be found in, e.g., Refs. [22, 52]. Here we only give a short outline. The method begins with the governing equation for the thermokinetic state [47]:

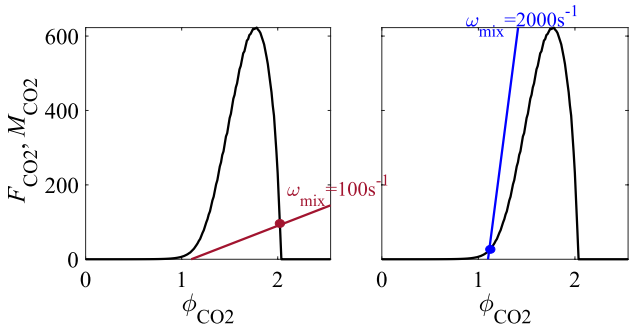

(a) process with one equilibrium state

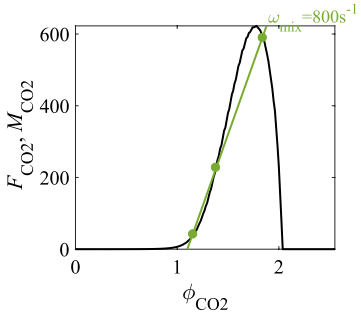

(b) process with three equilibrium states

Fig. 4 Illustration of stationary states for reaction and mixing processes with different turbulent frequency ω_{mix}. Black lines: reaction rate F_{CO2}; Color lines: mixing process M_{CO2}. Here parameters: $\phi_{\text{N2,mix}} = 25.27\text{mol/kg}$, $\phi_{\text{CO2,mix}} = 1.1\text{mol/kg}$ (color figure online)

$$\frac{\partial \Psi}{\partial t} = \mathbf{F}(\Psi) - \mathbf{u} \cdot \text{grad}(\Psi) + \frac{1}{\rho}\text{div}(\mathbf{D} \cdot \text{grad}(\Psi)) \tag{12}$$

Here, $\mathbf{u}$ is the velocity, $\mathbf{D}$ is the $n \times n$–dimensional transport matrix. According to Ref. [22], it was proposed that the REDIM can be obtained by integrating the following PDE system to its stationary solution:

$$\frac{\partial \Psi(\theta)}{\partial t} = \left(\mathbf{I} - \Psi_\theta \Psi_\theta^+\right) \cdot \left\{\mathbf{F} + \frac{1}{\rho}\left[\left(\mathbf{D}\Psi_\theta \chi\right)_\theta \chi\right]\right\} \tag{13}$$

where Θ is the reduced coordinate. Ψ_θ^+ is a pseudo-inverse and $\chi(\theta) = \text{grad}(\theta)$ is an estimate of the local gradients of the θ. The resulted REDIM reduced kinetic is then pre-tabulated as $\Psi = \Psi(\Theta)$.

4.2 Validation of the REDIMs for the laminar non-premixed counterflow flame configuration

A representative example of numerical computation of a laminar non-premixed counterflow flame (c.f. Section 2.2) is shown in Fig. 3. Here 3D REDIM reduced kinetics are

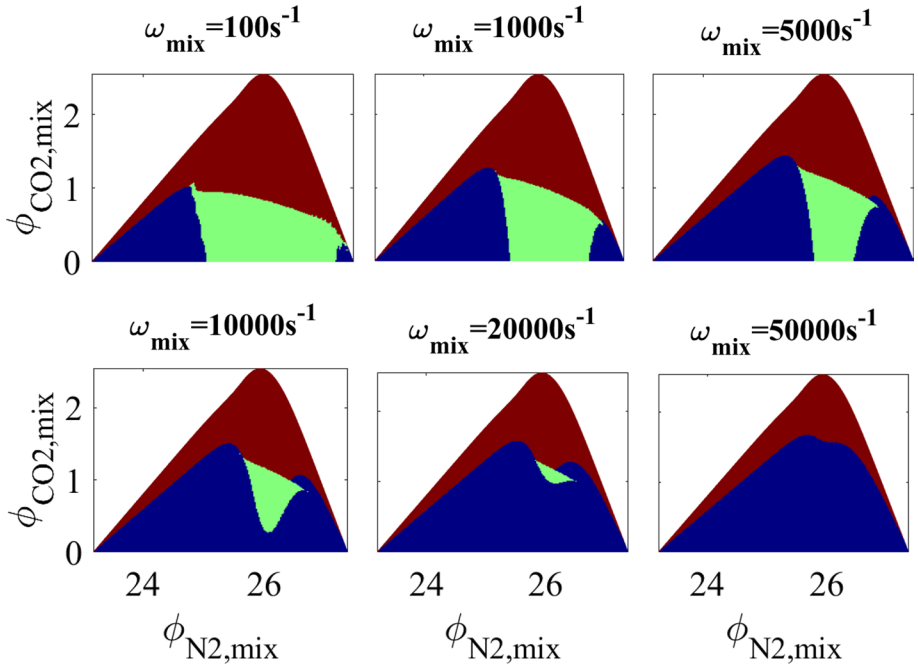

Fig. 5 Illustration on the properties of equilibrium states depending on the mixing states (shown as axis) and the turbulent frequency ω_{mix}

generated for each chemical mechanism. The solid lines represent the solution using the detailed chemistry, and the symbols represent the solution using the 3D REDIM models. Note that these 3D REDIM models, generated from different chemical mechanisms, will also be further used for the turbulence simulation.

We observe that the detailed solution and the REDIM solution correspond to each other with a high accuracy. The difference on the species concentration can be well captured by the REDIM model, and the extinction limit (most right point) is also predicted in a good accuracy. This is also consistent with the conclusions shown in, e.g., Ref. [53, 54]. A sensitivity analysis on the REDIM model with respect to the chemical mechanism can be made, based on Ref. [55], which is our ongoing research.

4.3 Application of the REDIM in the PDF modeling

For the application of the REDIM reduced kinetics for a turbulent simulation in the PDF model, the evolution of the reduced coordinate Θ is used instead of thermokinetic states Ψ:

$$\frac{\mathrm{d}\Psi^*}{\mathrm{d}t} = \Psi^+_\Theta \cdot \{\mathbf{F}(\Psi^*) + \mathbf{M}\}. \tag{14}$$

Using this equation, the reaction and mixing processes are projected on the REDIM manifold, and the evolution of the reduced coordinate is constrained on the manifold. For more discussion on the coupling of reduced kinetic and mixing processes, one can refer to Ref. [56].

5 Analysis on the interaction between mixing process and chemistry

Strong interaction between the chemical kinetics and mixing process poses whether one particle undergoes the burning process or the local extinction in the turbulent flames. Different chemical kinetics can lead to different degree of local extinction [1]. Therefore, it is worth investigating whether the mixing of one particle with others will lead to extinction or burning, provided that the reaction takes place at the same time. The analysis is based on the perfectly stirred reactor (PSR) model together with the reduced kinetics, which is expressed in the same form as Eq. (10):

$$\frac{\mathrm{d}\Theta}{\mathrm{d}t} = \mathbf{F}(\Theta) - \omega_{\text{mix}}\left(\Theta - \Theta_{\text{mix}}\right) \tag{15}$$

The corresponding stationary equilibrium state can be easily determined if the Θ_{eq} satisfies the following condition:

$$\mathbf{F}(\Theta_{\text{eq}}) = \omega_{\text{mix}}\left(\Theta_{\text{eq}} - \Theta_{\text{mix}}\right). \tag{16}$$

Note that one can get one equilibrium state or several equilibrium states, depending on the ω_{mix} and Θ_{mix}. Moreover,

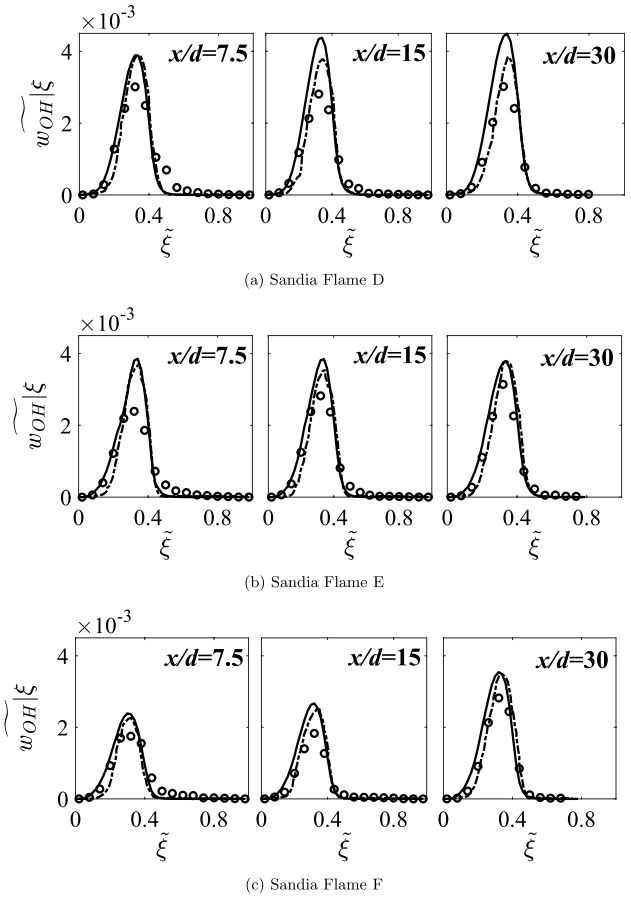

Fig. 6 Conditional Favre-averaged quantities over mixture fraction at three different locations for Sandia Flame D–F. Symbols: experimental measurements [23]; Dashed lines: ISAT results [1]; Solid lines: present results using 3D REDIM

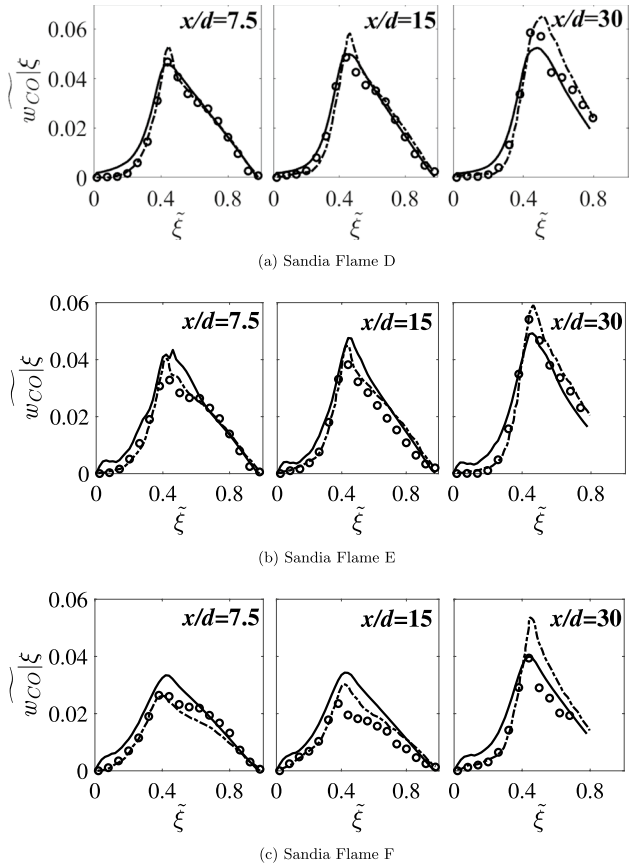

Fig. 7 Conditional Favre-averaged quantities over mixture fraction at three different locations for Sandia Flame D–F. Symbols: experimental measurements [23]; Dashed lines: ISAT results [1]; Solid lines: present results using 3D REDIM

the Θ_{eq} can fall into the steady flame regime (where steady burning flame exists) or the extinction regime (where no steady burning flame can be observed).

Figure 4 provides an illustrative example showing the stationary states. Here the study is based on a 2D REDIM reduced kinetics parameterized as $\Theta = (\phi_{N2}, \phi_{CO2})^T$. The mixing state in reduced coordinates in all three cases is the same: $\Theta_{mix} = (\phi_{N2,mix}, \phi_{CO2,mix})$=(25.27,1.1) mol/kg. The black lines represent the reaction rate for CO_2 (F_{CO2}), and the color lines the mixing rate (M_{CO2}) with three different turbulent mixing frequencies ω_{mix}. The circles stand for the corresponding equilibrium states for each case.

There are two different cases that can be observed and are needed to be addressed:

- Figure 4a: we observe that for both mixing processes with small and large turbulent frequencies $\omega_{mix} = 100$ and 2000 s^{-1}, only one stationary equilibrium state exists. On the left-hand side, reaction rate is larger than the mixing rate so that the change of state is positive. In contrast, right-hand state depicts that the mixing rate is larger than the reaction rate, and the change of state is negative. Therefore, this equilibrium state is a stable state, which does not depend on the initial conditions, and clarifies the direction the state change after mixing process (extinction or ignited). Moreover, if the turbulent frequency is small (here $\omega_{mix} = 100\,s^{-1}$), the equilibrium state falls into the burning regime where steady burning flame exists, due to the reaction being much faster; and the equilibrium state falls into the extinction regime where no steady burning flame exists and quenching takes place, if the turbulent frequency is large (here $\omega_{mix} = 2000\,s^{-1}$).
- Figure 4b: at moderate turbulent frequency (here $\omega_{mix} = 800\,s^{-1}$), three stationary equilibrium states exist, in which one is an unstable state. Depending on the initial state, its corresponding equilibrium state can fall into either the burning regime (right one) or the flame extinction regime (left one).

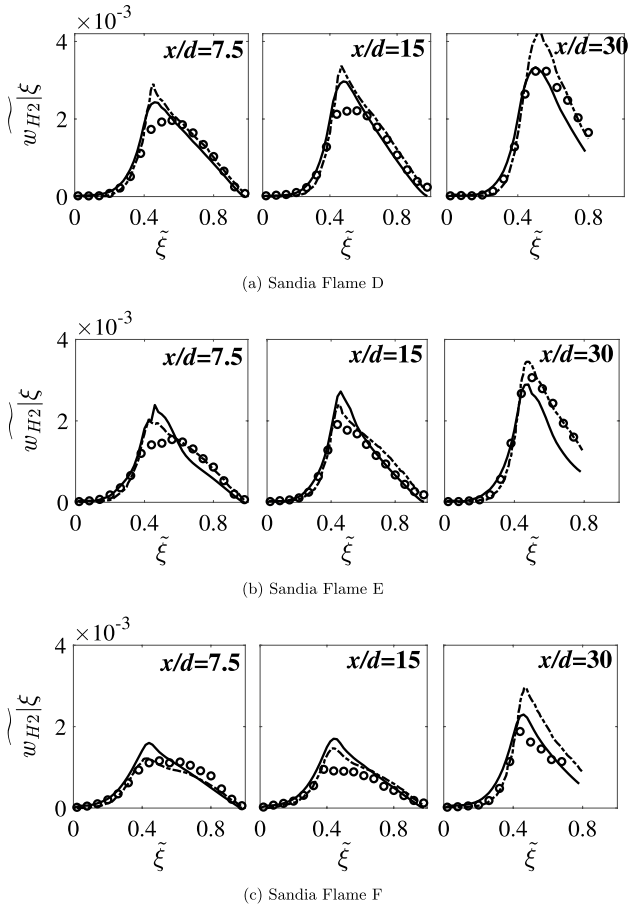

Fig. 8 Conditional Favre-averaged quantities over mixture fraction at three different locations for Sandia Flame D–F. Symbols: experimental measurements [23]; Dashed lines: ISAT results [1]; Solid lines: present results using 3D REDIM

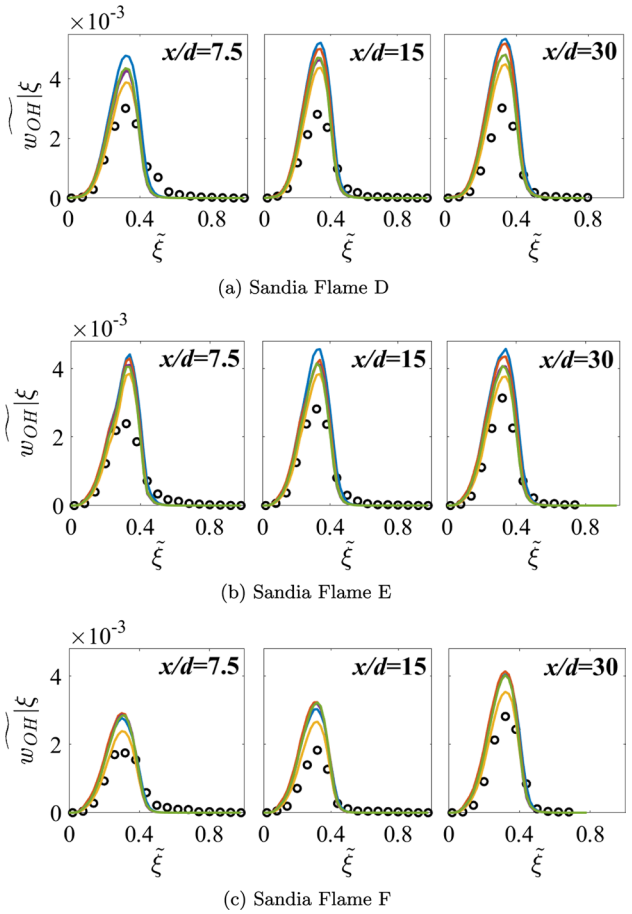

Fig. 9 Conditional Favre-averaged mass fraction of OH over mixture fraction at three different locations for Sandia Flame D–F. Symbols: experimental measurements [23]; Colors lines are the same as those in Fig. 1 (color figure online)

Figure 5 shows several representative examples about how the stationary equilibrium state changes with the turbulent frequency, depending on different mixing states. Three different regimes are observed:

- *Red regime:* only one stable equilibrium state is observed (c.f. Figure 4a, left) and the reaction rate is observed to be much larger than the mixing rate, such that this equilibrium state falls in the burning regime.
- *Blue regime:* in this regime, only one stable equilibrium state is observed (c.f. Figure 4a, right). The reaction rate is much smaller than the mixing rate and equilibrium state falls in the extinction regime.
- *Green regime:* in this case, three equilibrium states are observed (c.f. Figure 4b). Depending on the initial state, the equilibrium state can fall into either the burning regime or the extinction regime.

It is quite evident that at a low turbulent mixing frequency (here, e.g., $\omega_{\text{mix}} = 100\,\text{s}^{-1}$) the extinction is more likely to happen at lean and rich side where chemical reaction is very slow, and most of the regime shows that the equilibrium state falls into the burning regime as the reaction is much faster as compared to the mixing process at a low turbulent mixing frequency. Nevertheless, the blue regime expands because the mixing process becomes faster and overcomes the reaction rate. At extremely high turbulent mixing frequency (here, e.g., $\omega_{\text{mix}} = 50,000\,\text{s}^{-1}$), green regime disappears and the blue regimes covers most of the part, indicating that at high turbulent intensity the mixing process becomes so fast that particle states have a high tendency to fall in the extinction regime.

This analysis clearly helps us to examine the interaction between mixing process and chemical reactions. Later, the influence of the key elementary reactions on the properties of equilibrium state will be discussed.

However, it should be emphasized that this analysis does not demonstrate how fast the thermokinetic states can reach their equilibrium states after mixing, instead they explain the direction in which they will arrive.

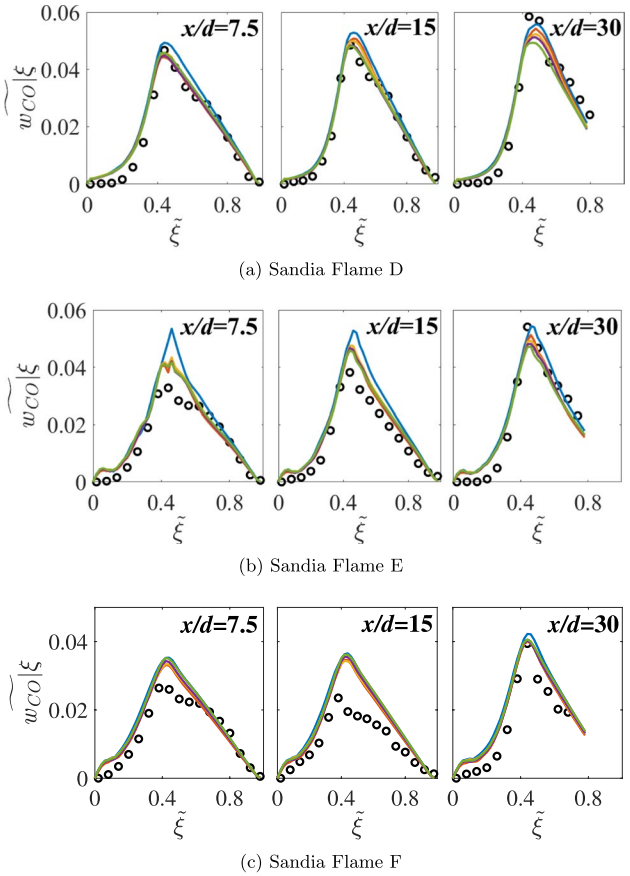

Fig. 10 Conditional Favre-averaged mass fraction of CO over mixture fraction at three different locations for Sandia Flame D–F. Symbols: experimental measurements [23]; Colors lines are the same as those in Fig. 1 (color figure online)

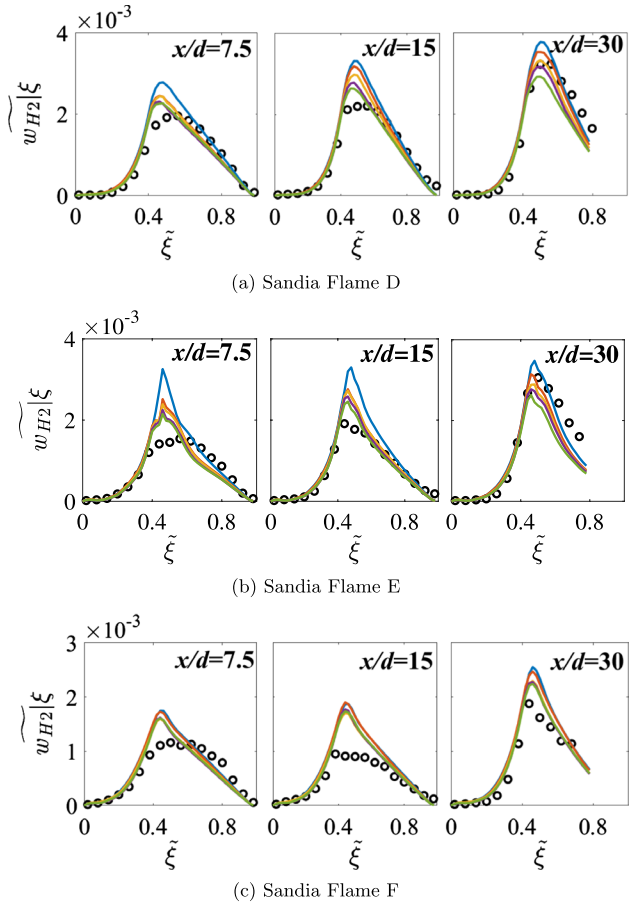

Fig. 11 Conditional Favre-averaged mass fraction of H_2 over mixture fraction at three different locations for Sandia Flame D–F. Symbols: experimental measurements [23]; Colors lines are the same as those in Fig. 1 (color figure online)

6 Computational test case and a-priori validation

6.1 Configuration of Sandia flame series

In order to compare the performance of different methane mechanisms on the turbulent reacting flames, the well-known methane/air piloted turbulent jet non-premixed flame [23], Sandia Flame series D–F, is chosen as test case. This flame is optimal for our purpose because the Reynolds number of the jet increases from 22,400 (Sandia Flame D) to 44,800 (Sandia Flame F), ranging from low to high degree of local extinction. It can be used not only to investigate the difference on the prediction of species concentration, but also to study the predicted local extinction.

6.2 *A-priori* validation

The hybrid CFD/transported-PDF method using the REDIM reduced kinetics has been developed and successfully applied for the simulation of the Sandia Flame in our previous work [32, 56] by using the GRI 3.0 mechanism. The aim of this part is show that our applied algorithm based on the 3D REDIM reduced chemistry provides the similar results as those based on the detailed chemistry calculation.

We show in Figs. 6, 7, 8 the present numerical results (solid lines) together with experimental measurement (symbols) [23] and the results based on ISAT detailed chemistry (dashed lines) [1] for Sandia Flame D,E and F. It can be clearly observed that the present hybrid model using the REDIM reduced kinetics agree with those using the ISAT detailed kinetics very good for all represented species. Compared with the experimental measurements [23], numerical simulations show large deviations for H_2 species, especially at positions $x/d = 7.5$ and 15. This can be attributed to the fact that the differential diffusion effect of H_2 at both positions is dominant and the unity Lewis number assumption is not accurate enough for the prediction of H_2 concentration [32, 57].

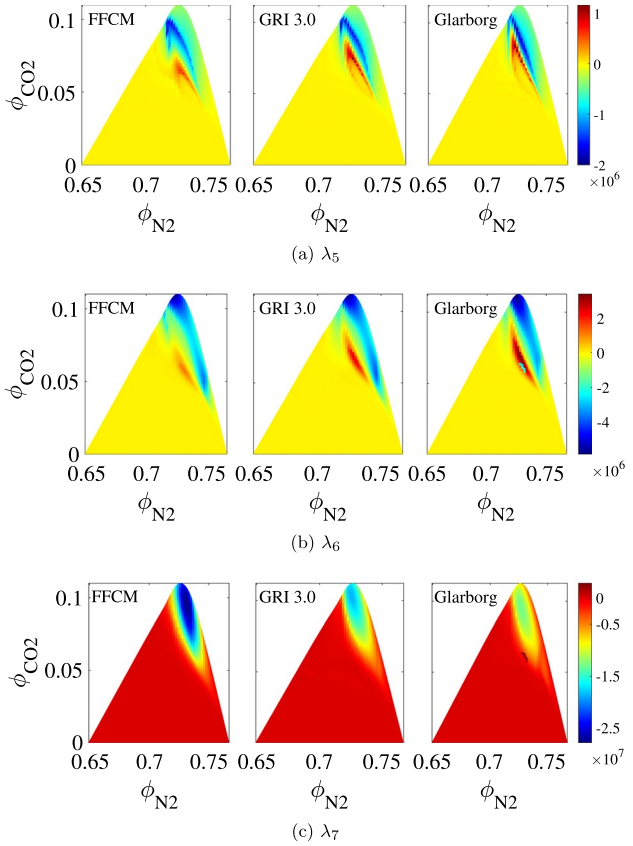

Fig. 12 The eigenvalues ($|\lambda_5| < |\lambda_6| < |\lambda_7|$) along the 2D REDIM composition state space

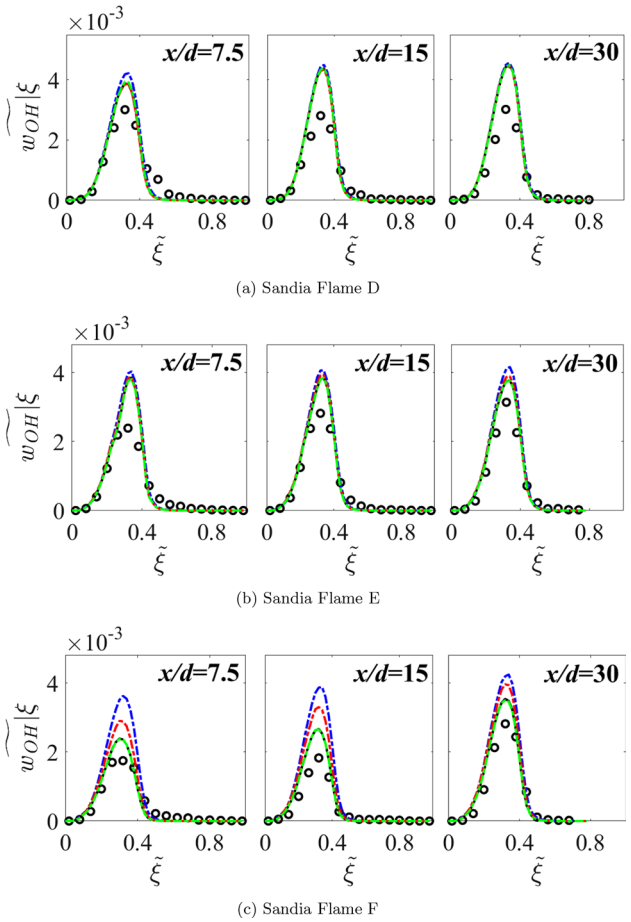

Fig. 13 Conditional Favre-averaged mass fraction of OH over mixture fraction at three different locations for Sandia Flame D–F with the change of the pre-exponent factor of three different elementary reactions. Symbols: experimental measurements [23]; Colors lines are the same as those in Fig. 2 (color figure online)

To be concluded, the present hybrid model using the 3D REDIM reduced kinetics can predict the local extinction and re-ignition effect accurately and has almost the similar performance as those using the detailed chemistry. Therefore, the use of REDIM model does not introduce additional model errors.

In the following, 3D REDIM reduced kinetics will be generated for each chemical mechanism. Its performance on the prediction of (i) species profiles under different strain rates, (ii) the extinction limit and (iii) the transient extinction solutions are examined for the laminar non-premixed flame.

7 Results and discussion

This section is divided as follows. First of all, selected species concentration profiles for the Sandia Flame Series D-F are used to analyze the behavior of five different chemical kinetics. Secondly, the influence of reaction rates is studied side by side and discussed together with the laminar flame calculation.

7.1 Comparison of different chemical mechanism for Sandia flame series

Numerical simulations are performed by using five different chemical mechanisms listed in Table 2 for Sandia Flame series D - F at three different axial locations, i.e., x/d = 7.5,15 and 30. The following observations can be pointed out as follows:

- All five chemical mechanisms provide very similar results and agree very well with the experimental measurements [23].
- For Sandia Flame D and E where the degree of local extinction is low till moderate, the differences of species concentrations observed in the laminar calculation (c.f. Figure 1) are also preserved in the turbulent calculation.

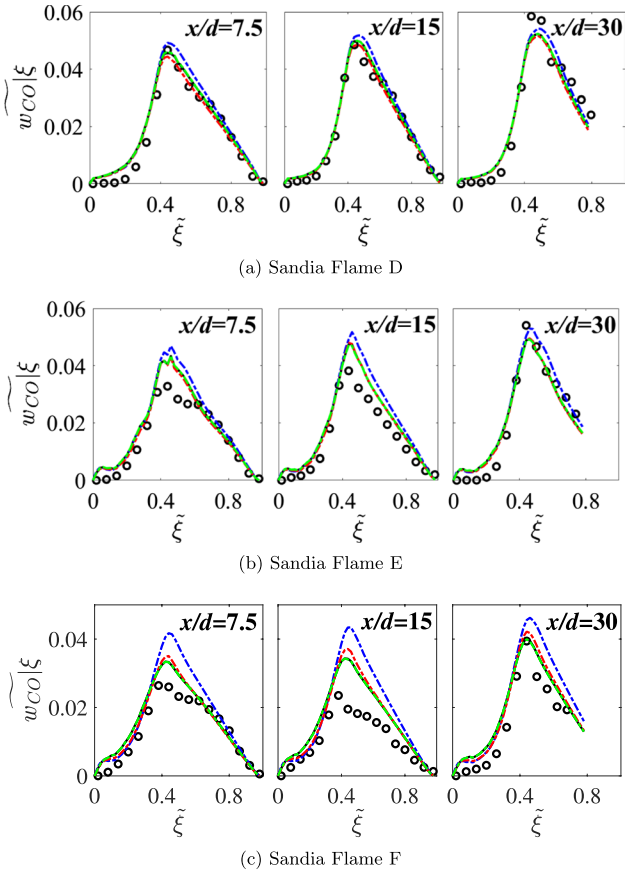

Fig. 14 Conditional Favre-averaged mass fraction of CO over mixture fraction at three different locations for Sandia Flame D, E and F with the change of the pre-exponent factor of three different elementary reactions. Symbols: experimental measurements [23]; Colors lines are the same as those in Fig. 2 (color figure online)

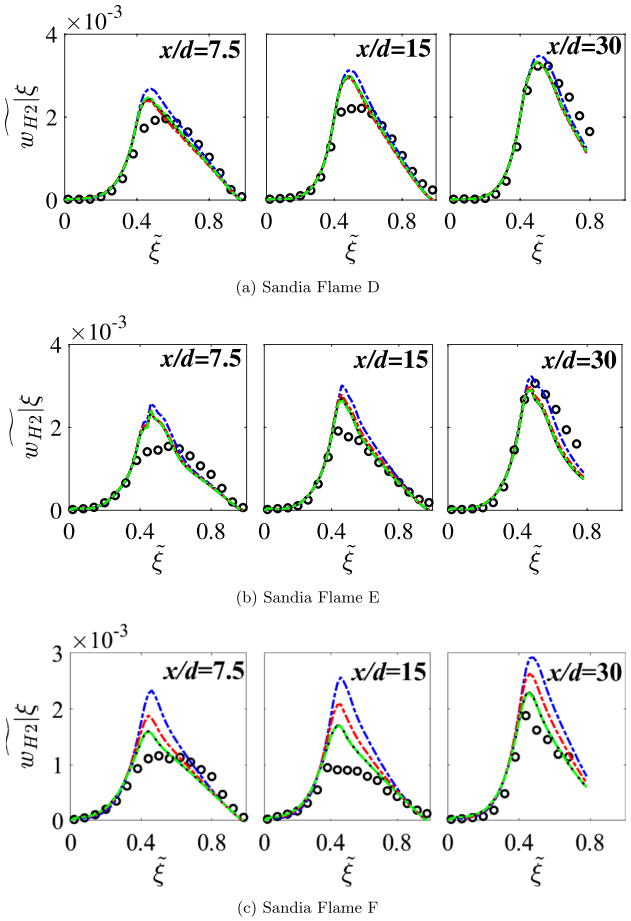

Fig. 15 Conditional Favre-averaged mass fraction of H_2 over mixture fraction at three different locations for Sandia Flame D–F with the change of the pre-exponent factor of three different elementary reactions. Symbols: experimental measurements [23]; colors lines are the same as those in Fig. 2 (color figure online)

For example, FFCM mechanism predicts the highest level of CO concentration due to its highest formation rate of CO, which can be noticed in both cases.

- A high degree of local extinction can be observed for the Sandia Flame F, the differences in the concentrations of the predicted species become trivial. It can be deduced that at high turbulence, the turbulent mixing process plays a more important role in the numerical accuracy, and leading to the suppression of slight differences in the species concentration. Another most important aspect is the accuracy in the prediction of extinction limit. Since all five chemical mechanisms have the similar extinction limit (the most right point in Fig. 1), all mechanisms predict the same levels of local extinction. Further ahead, it will be shown that how the degree of local extinction can be under-estimated, if the reaction rates of some key elementary reactions are changed and the corresponding extinction limits in the laminar calculation are changed (Figs. 9, 10, 11).

The similarity in the predicted species concentrations depicts that the chemical source terms are of the similar order of magnitude despite of different chemical mechanisms. In order to examine this issue, the eigenvalues of the local Jacobi of the chemical source terms are calculated for the FFCM, GRI 3.0 and Glarborg mechanisms. These eigenvalues correspond to the inverse of the characteristic chemical time-scales, describing how fast the chemical reaction is. In Fig. 12, the first three eigenvalues ($|\lambda_5| < |\lambda_6| < |\lambda_7|$) along the 2D REDIM composition state space are shown. The use of 2D REDIM is only for the purpose of simple

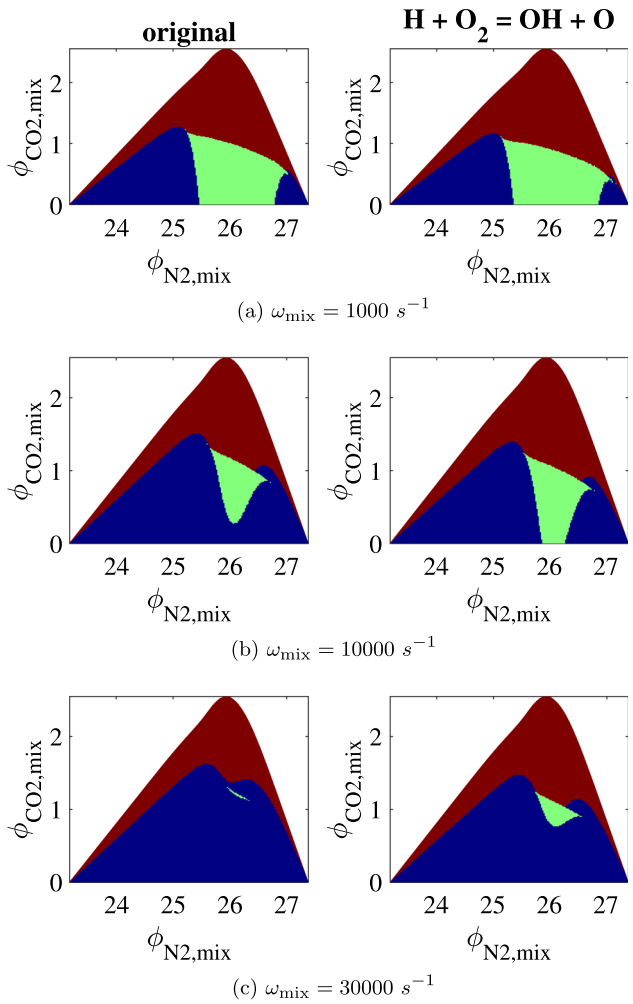

Fig. 16 Properties of equilibrium states for left) unchanged elementary reactions and right) the change of reaction rate of (R1) $H + O_2 = OH + O$ by 20%

representation. The same conclusion can be observed for a 3D REDIM used here. The first four eigenvalues ($|\lambda_i|$ for $i \leq 4$) represents the infinite long time-scales due to conservation of elements and are negligible.

We observe clearly that the eigenvalues in the composition state are very similar by using these three chemical mechanisms. This signifies the below points:

- Although the elementary reactions in different chemical mechanisms can largely differ from each other, the chemical source terms of the species are of the similar order of magnitude and the formation/consumption of species are similarly fast. Therefore, these five chemical mechanisms show similar prediction for the species concentrations.
- Since the chemical time-scales are at the similar order of magnitude, the systems using different chemical mechanisms should have the similar dynamic behaviors. In other words, the response of the combustion phenomena to the physical perturbation (e.g., turbulent mixing process) is similar and results in the indistinguishable level of degree of local extinction.

7.2 Sensitivity with respect to the chemical kinetics

In this section, observations from the laminar configuration are compared and discussed together with those from the turbulent configuration by numerically simulating the Sandia Flame series. Figures 13, 14 and 15 show the predicted species mass fractions against mixture fraction, if each elementary reaction has a 20% higher pre-exponential factor. The GRI 3.0 is used here as base chemical mechanism for the investigation.

While the Sandia Flames D &E are less sensitive to the change of selected elementary reactions, the Sandia Flame F is significantly influenced by their reaction rates. It is observed that an increase in reaction rate of (R1) $H + O_2 = OH + O$ leads to a large over-prediction of all the species concentration, while an increase in reaction rate of (R3) $CH + OH = HCO + H$ does not change the numerical predictions. This is very much consistent with the observation from the laminar case, i.e., the (R1) is most important for the prediction of the extinction limit. An increase in extinction limit means a lower degree of local extinction.

Since the chemical kinetics play an important role in the prediction of local extinction, the interaction between chemical kinetics and mixing process is investigated. Figure 16 shows the properties of equilibrium states at three different turbulent mixing frequencies spanning from low ($\omega_{\text{mix}} = 1000\,\text{s}^{-1}$) to high ($\omega_{\text{mix}} = 30,000\,\text{s}^{-1}$) levels. In the left column, we show the results obtained using the original unchanged chemical kinetics, and in the right by changing the reaction rate of (R1) $H + O_2 = OH + O$ by 20%. It is evident that while the properties of equilibrium states are not that much sensitive to the chemical reaction, they become increasingly sensitive with higher ω_{mix}. For example, at $\omega_{\text{mix}} = 30,000\,\text{s}^{-1}$, the properties using the original chemical kinetics show larger area of extinction regime (blue regime) and the green regime where three equilibrium states almost disappear. This confirms the statement that the increase of reaction rate of (R1) $H + O_2 = OH + O$ by 20% will lead to a lower degree of local extinction and a more stable flame.

8 Conclusions

In the present work, five different chemical mechanisms for the CH_4 combustion system are applied for the numerical simulation of the Sandia Flame D - F, in which the degree

of local extinction varies from low to high levels. The turbulence simulation is based on the CFD/transported-PDF method and the reaction–diffusion manifolds (REDIMs) are used to speed up the numerical computation. It is shown that all five chemical mechanisms provide the similar prediction of species concentration and agree with the experimental measurements very well. An analysis on the chemical timescales indicates that the chemical source terms are of the similar order of magnitude and thus the similar formation rate of the species among these chemical kinetics.

Further sensitivity analysis shows that the degree of local extinction is very sensitive to (R1) $H + O_2 = OH + O$ and (R2) $CO + OH = CO_2 + H$. An increase of reaction rates of both elementary reactions improves the flame stability against extinction and thus leads to an over-prediction of the species concentrations.

The chemical mechanisms are also suggested to be performed for more complex combustion systems such as multi-regime turbulent combustion.

Acknowledgements The authors C. Yu and U. Maas gratefully acknowledge financial support from the German Research Foundation (Deutsche Forschungsgemeinschaft, DFG)—Projektnummer 237267381—TRR 150, subprojects B06 and B07. The work of L.Cai was supported by the Fundamental Research Funds for the Central Universities. F. Minuzzi acknowledges Office of Naval Research Global—ONR-USA, under the contract No. N629091812124.

Author Contributions C. Yu, L. Cai, F. Minuzzi did conceptualization; C. Yu, L. Cai, F. Minuzzi and U. Maas done methodology; C. Yu, L. Chopra contributed to software and simulations; C. Yu, L. Chopra validated the study; C. Yu, L. Cai, F. Minuzzi and U. Maas analyzed the data; C. Yu was involved in writing—original draft preparation; C. Yu, L. Cai, L. Chopra, F. Minuzzi and U. Maas done writing—review and editing; C. Yu supervised the study and administrated the project. All authors have reviewed the manuscript.

Funding Open Access funding enabled and organized by Projekt DEAL.

Declarations

Conflict of interest The authors declare that they have no conflict of interest.

Open Access This article is licensed under a Creative Commons Attribution 4.0 International License, which permits use, sharing, adaptation, distribution and reproduction in any medium or format, as long as you give appropriate credit to the original author(s) and the source, provide a link to the Creative Commons licence, and indicate if changes were made. The images or other third party material in this article are included in the article's Creative Commons licence, unless indicated otherwise in a credit line to the material. If material is not included in the article's Creative Commons licence and your intended use is not permitted by statutory regulation or exceeds the permitted use, you will need to obtain permission directly from the copyright holder. To view a copy of this licence, visit http://creativecommons.org/licenses/by/4.0/.

References

1. Cao RR, Pope SB (2005) The influence of chemical mechanisms on pdf calculations of nonpremixed piloted jet flames. Combust Flame 143(4):450–470
2. Curran HJ (2019) Developing detailed chemical kinetic mechanisms for fuel combustion. Proc Combust Inst 37(1):57–81
3. Westbrook CK, Pitz WJ, Herbinet O, Curran HJ, Silke EJ (2009) A comprehensive detailed chemical kinetic reaction mechanism for combustion of n-alkane hydrocarbons from n-octane to n-hexadecane. Combust Flame 156(1):181–199
4. Dasgupta D, Sun W, Day M, Lieuwen T (2017) Effect of turbulence-chemistry interactions on chemical pathways for turbulent hydrogen-air premixed flames. Combust Flame 176:191–201
5. Smooke M, Puri I, Seshadri K (1988) A comparison between numerical calculations and experimental measurements of the structure of a counterflow diffusion flame burning diluted methane in diluted air. In: Symposium (International) on Combustion, vol 21. Elsevier, pp 1783–1792
6. Farokhi M, Birouk M, Tabet F (2017) A computational study of a small-scale biomass burner: the influence of chemistry, turbulence and combustion sub-models. Energy Convers Manage 143:203–217
7. Zhang P, Zsély IG, Samu V, Nagy T, Turányi T (2021) Comparison of methane combustion mechanisms using shock tube and rapid compression machine ignition delay time measurements. Energy Fuels 35(15):12329–12351
8. Zhang P, Zsély IG, Papp M, Nagy T, Turányi T (2022) Comparison of methane combustion mechanisms using laminar burning velocity measurements. Combust Flame 238:111867
9. Bougrine S, Richard S, Nicolle A, Veynante D (2011) Numerical study of laminar flame properties of diluted methane-hydrogen-air flames at high pressure and temperature using detailed chemistry. Int J Hydrog Energy 36(18):12035–12047
10. Cai L, Kruse S, Felsmann D, Pitsch H (2021) A methane mechanism for oxy-fuel combustion: extinction experiments, model validation, and kinetic analysis. Flow Turbul Combust 106(2):499–514
11. Wang Y, Movaghar A, Wang Z, Liu Z, Sun W, Egolfopoulos FN, Chen Z (2020) Laminar flame speeds of methane/air mixtures at engine conditions: performance of different kinetic models and power-law correlations. Combust Flame 218:101–108
12. Su J, Wu Y, Wang Y, Chen X, Chen Z (2021) Skeletal and reduced kinetic models for methane oxidation under engine-relevant conditions. Fuel 288:119667
13. Roomina M, Bilger R (2001) Conditional moment closure (CMC) predictions of a turbulent methane-air jet flame. Combust Flame 125(3):1176–1195
14. Luca S, Al-Khateeb AN, Attili A, Bisetti F (2018) Comprehensive validation of skeletal mechanism for turbulent premixed methane-air flame simulations. J Propul Power 34(1):153–160
15. Gao X, Duan F, Lim SC, Yip MS (2013) Nox formation in hydrogen-methane turbulent diffusion flame under the moderate or intense low-oxygen dilution conditions. Energy 59:559–569
16. Mikulčić H, Baleta J, Wang X, Wang J, Qi F, Wang F (2021) Numerical simulation of ammonia/methane/air combustion using reduced chemical kinetics models. Int J Hydrog Energy 46(45):23548–23563
17. Smith GP, Tao Y, Wang H (2016) Foundational fuel chemistry model version 1.0 (FFCM-1). http://nanoenergy.stanford.edu/ffcm1. Accessed Dec 2021
18. Smith GP (1999) Gri-mech 3.0. http://www.me.berkley.edu/gri_mech/
19. Mechanical, Aerospace Engineering (Combustion Research), U.o.C.a.S.D.: Chemical-kinetic mechanisms for combustion

applications. https://web.eng.ucsd.edu/mae/groups/combustion/mechanism.html
20. Wang H, You X, Joshi AV, Davis SG, Laskin A, Fokion E, Law CK (2007) Usc mech version ii. high-temperature combustion reaction model of h2/co/c1-c4 compounds. http://ignis.usc.edu/USC_Mech_II.htm
21. Glarborg P, Miller JA, Ruscic B, Klippenstein SJ (2018) Modeling nitrogen chemistry in combustion. Prog Energy Combust Sci 67:31–68
22. Bykov V, Maas U (2007) The extension of the ILDM concept to reaction-diffusion manifolds. Combust Theor Model 11(6):839–862
23. Barlow R, Frank J (1998) Effects of turbulence on species mass fractions in methane/air jet flames. In: Symposium (international) on combustion, vol 27. Elsevier, pp 1087–1095
24. Bell JB, Cheng RK, Day MS, Shepherd IG (2007) Numerical simulation of Lewis number effects on lean premixed turbulent flames. Proc Combust Inst 31(1):1309–1317
25. Peters N (2001) Turbulent combustion. IOP Publishing
26. Maas U, Warnatz J (1988) Ignition processes in hydrogen-oxygen mixtures. Combust Flame 74(1):53–69
27. Tomlin AS, Turányi T (2013) Investigation and improvement of reaction mechanisms using sensitivity analysis and optimization. In: Cleaner combustion. Springer, pp 411–445
28. Eckart S, Yu C, Maas U, Krause H (2021) Experimental and numerical investigations on extinction strain rates in non-premixed counterflow methane and propane flames in an oxygen reduced environment. Fuel 298:120781
29. Vagelopoulos CM, Egolfopoulos FN (1998) Direct experimental determination of laminar flame speeds. In: Symposium (international) on combustion, vol 27. Elsevier, pp 513–519
30. Vagelopoulos CM, Egolfopoulos FN, Law CK (1994) Further considerations on the determination of laminar flame speeds with the counterflow twin-flame technique. In: Symposium (international) on combustion, vol 25. Elsevier, pp 1341–1347
31. Jenny P, Pope SB, Muradoglu M, Caughey DA (2001) A hybrid algorithm for the joint pdf equation of turbulent reactive flows. J Comput Phys 166(2):218–252
32. Yu C, Breda P, Minuzzi F, Pfitzner M, Maas U (2021) A novel model for incorporation of differential diffusion effects in pdf simulations of non-premixed turbulent flames based on reaction-diffusion manifolds (redim). Phys Fluids 33(2):025110
33. Muradoglu M, Pope SB, Caughey DA (2001) The hybrid method for the pdf equations of turbulent reactive flows: consistency conditions and correction algorithms. J Comput Phys 172(2):841–878
34. Pope SB, Pope SB (2000) Turbulent flows. Cambridge University Press
35. Pope SB (1985) Pdf methods for turbulent reactive flows. Prog Energy Combust Sci 11(2):119–192
36. Haworth DC (2010) Progress in probability density function methods for turbulent reacting flows. Prog Energy Combust Sci 36(2):168–259
37. Subramaniam S, Pope S (1998) A mixing model for turbulent reactive flows based on Euclidean minimum spanning trees. Combust Flame 115(4):487–514
38. Klimenko AY, Pope S (2003) The modeling of turbulent reactive flows based on multiple mapping conditioning. Phys Fluids 15(7):1907–1925
39. Celis C, Silva LF (2015) Lagrangian mixing models for turbulent combustion: review and prospects. Flow Turbul Combust 94(3):643–689
40. Fox RO (2003) Computational models for turbulent reacting flows. Cambridge University Press
41. Van Slooten P, Jayesh Pope S (1998) Advances in PDF modeling for inhomogeneous turbulent flows. Phys Fluids 10(1):246–265
42. Wang H, Hawkes ER, Zhou B, Chen JH, Li Z, Aldén M (2017) A comparison between direct numerical simulation and experiment of the turbulent burning velocity-related statistics in a turbulent methane-air premixed jet flame at high Karlovitz number. Proc Combust Inst 36(2):2045–2053
43. Aspden A, Bell J, Day M, Egolfopoulos F (2017) Turbulence-flame interactions in lean premixed dodecane flames. Proc Combust Inst 36(2):2005–2016
44. Carlsson H, Yu R, Bai X-S (2014) Direct numerical simulation of lean premixed ch4/air and h2/air flames at high Karlovitz numbers. Int J Hydrog Energy 39(35):20216–20232
45. Yenerdag B, Naka Y, Shimura M, Tanahashi M (2015) 3d DNS of methane-air turbulent premixed flame in thin reaction zones with a detailed kinetic mechanism. In: 9th international symposium on turbulence and shear flow phenomena. Begel House Inc
46. Maas U, Tomlin AS (2013) Time-scale splitting-based mechanism reduction. In: Cleaner combustion. Springer, pp 467–484
47. Goussis DA, Maas U (2011) Model reduction for combustion chemistry. In: Turbulent combustion modeling. Springer, pp 193–220
48. Maas U, Pope SB (1992) Implementation of simplified chemical kinetics based on intrinsic low-dimensional manifolds. In: Symposium (international) on combustion, vol 24. Elsevier, pp 103–112
49. Peters N (1984) Laminar diffusion flamelet models in non-premixed turbulent combustion. Prog Energy Combust Sci 10(3):319–339
50. Van Oijen J, De Goey L (2002) Modelling of premixed counterflow flames using the flamelet-generated manifold method. Combust Theor Model 6(3):463
51. Pope SB (1997) Computationally efficient implementation of combustion chemistry using in situ adaptive tabulation. Combust Theor Model 1(1):41–63
52. Golda P, Blattmann A, Neagos A, Bykov V, Maas U (2020) Implementation problems of manifolds-based model reduction and their generic solution. Combust Theor Model 24(3):377–406
53. Yu C, Li X, Wu C, Neagos A, Maas U (2020) Automatic construction of redim reduced chemistry with a detailed transport and its application to ch4 counterflow flames. Energy Fuels 34(12):16572–16584
54. Yu C, Minuzzi F, Maas U (2020) Redim reduced chemistry for the simulation of counterflow diffusion flames with oscillating strain rates. Combust Theor Model 24(4):682–704
55. Yu C, Maas U (2022) Sensitivity of reaction-diffusion manifolds (redim) method with respect to the gradient estimate. Combust Theory Model 26(3):1–31
56. Yu C, Breda P, Pfitzner M, Maas U (2021) Coupling of mixing models with manifold based simplified chemistry in pdf modeling of turbulent reacting flows. Proc Combust Inst 38(2):2645–2653
57. Wang H, Kim K (2015) Effect of molecular transport on pdf modeling of turbulent non-premixed flames. Proc Combust Inst 35(2):1137–1145

Publisher's Note Springer Nature remains neutral with regard to jurisdictional claims in published maps and institutional affiliations.